Journal of Materials Science: Materials in Medicine (2020)31:100
https://doi.org/10.1007/s10856-020-06439-w

DELIVERY SYSTEMS

Original Research

ZnO-mesoporous glass scaffolds loaded with osteostatin and mesenchymal cells improve bone healing in a rabbit bone defect

D. Lozano[1,2] · J. Gil-Albarova[3,4] · C. Heras[1] · S. Sánchez-Salcedo[1,2] · V. E. Gómez-Palacio[3] · A. Gómez-Blasco[3] · J. C. Doadrio[1] · M. Vallet-Regí[1,2] · A. J. Salinas[1,2]

Received: 19 March 2020 / Accepted: 24 September 2020

Abstract

The use of 3D scaffolds based on mesoporous bioactive glasses (MBG) enhanced with therapeutic ions, biomolecules and cells is emerging as a strategy to improve bone healing. In this paper, the osteogenic capability of ZnO-enriched MBG scaffolds loaded or not with osteostatin (OST) and human mesenchymal stem cells (MSC) was evaluated after implantation in New Zealand rabbits. Cylindrical meso-macroporous scaffolds with composition (mol %) $82.2SiO_2$–$10.3CaO$–$3.3P_2O_5$–$4.2ZnO$ (4ZN) were obtained by rapid prototyping and then, coated with gelatin for easy handling and potentiating the release of inorganic ions and OST. Bone defects (7.5 mm diameter, 12 mm depth) were drilled in the distal femoral epiphysis and filled with 4ZN, 4ZN + MSC, 4ZN + OST or 4ZN + MSC + OST materials to evaluate and compare their osteogenic features. Rabbits were sacrificed at 3 months extracting the distal third of bone specimens for necropsy, histological, and microtomography (μCT) evaluations. Systems investigated exhibited bone regeneration capability. Thus, trabecular bone volume density (BV/TV) values obtained from μCT showed that the good bone healing capability of 4ZN was significantly improved by the scaffolds coated with OST and MSC. Our findings in vivo suggest the interest of these MBG complete systems to improve bone repair in the clinical practice.

Graphical Abstract

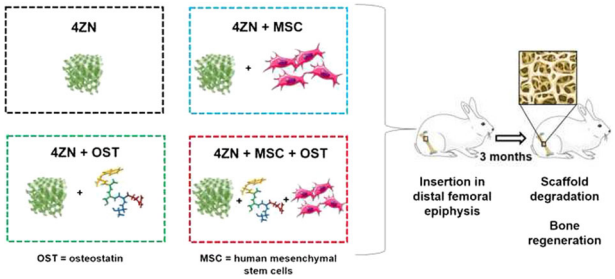

1 Introduction

In a bone damage scenario, bone repair is a spontaneous process which takes place in physiological circumstances. However, there are some clinical situations in which this process may not be sufficient. In those cases, bone repair

Supplementary information The online version of this article (https://doi.org/10.1007/s10856-020-06439-w) contains supplementary material, which is available to authorized users.

✉ J. Gil-Albarova
jgilalba@unizar.es

✉ A. J. Salinas
salinas@ucm.es

[1] Department of Chemistry in Pharmaceutical Sciences, Universidad Complutense, UCM; Instituto Investigación Sanitaria Hospital 12 de Octubre, imas12, Madrid, Spain

[2] Networking Research Center on Bioengineering, Biomaterials and Nanomedicine (CIBER-BBN), Madrid, Spain

[3] Servicio de Cirugía Ortopédica y Traumatología, Hospital Universitario Miguel Servet, Zaragoza, Spain

[4] Departamento de Cirugía. Facultad de Medicina, Universidad de Zaragoza, Zaragoza, Spain

Published online: 31 October 2020

can be achieved by bone engineering [1–3]. During the last years, mesoporous bioactive glasses (MBGs) based on SiO_2–CaO–P_2O_5 have arisen as exceptional material to develop scaffolds which constitute a perfect tool for this purpose. The description that certain glasses, in the SiO_2–CaO–P_2O_5–Na_2O system, could chemically bond with bone was first reported in 1971 [4]. These glasses often denoted as bioglasses, obtained by quenching of a melt, attained the FDA clearance in 1985 to be used for replacement of the middle ear ossicles and later on for other maxillofacial and dental applications including the treatment of periodontal disease. In 2000, bioglasses were approved for orthopaedics bone grafts in non-load bearing sites, which is the application that will be explored in this paper. Moreover, in 2004 they were approved for the treatment of dentinal hypersensitivity. In the last decades, many researches were conducted in this area following a double way. On the one hand, new applications of bioactive glasses were sought outside the skeletal system like the peripheral nerve repair, wound healing and many others including the cancer treatment. On the other, it was seeking to improve their performance in the body with new methods of synthesis that lead to porous materials, sol-gel glasses [5] and to obtain them with huge ordered mesoporosity using surfactants as templates [6]. These new methods of synthesis yield to glasses more reactive than traditional ones that exhibited the extra capability to be loaded with osteogenic substances that can be released in a controlled way. The emergence of bone tissue engineering confirmed that biomaterials by themselves, in this case the glasses were not enough for an accurate treatment of bone defects.

In this sense, MBGs present bone regenerative properties and high order mesoporous structures which are able to load and release bone tissue promoting agents [1, 2, 7, 8]. MBGs also presents huge surface area and pore volume what causes quicker in vitro responses than other bioactive materials [7, 9]. Besides, MBG degradation increases intracellular ion concentration of their basics constituents, i.e., Si (IV), Ca^{2+} and P (V) which could lead to the activation of bone regeneration intracellular signaling pathways [10, 11]. Moreover, MBGs bone regeneration features can be enhanced by the addition of certain inorganic ions with biological activity such as Cu^{2+}, Mg^{2+}, Ce^{3+}, Co^{2+}, Ga^{3+}, Sr^{2+} or Zn^{2+}. In this regard, Zn^{2+} ions, showed good properties, due to their specific capacity to increase osteogenesis [12], angiogenesis [1, 12], and their antimicrobial properties [12, 13].

One of the most promising strategies under investigation to improve bone healing implicates the use of the scaffolds in combination with human mesenchymal stem cells (MSC) and osteogenic and angiogenic factors, such as parathyroid hormone (PTH)-related protein, PTHrP. This protein contains an N-terminal 1–37 fragment that is similar to PTH and a C-terminal region (not homologous to PTH), containing 107–111 sequence (osteostatin, OST) [14]. This family of peptides has been shown to modulate bone metabolism. For instance, N-terminal PTHrP analogs have shown to enhance bone metabolic pathways in humans and rodents upon systemic intermittent administration [15–17]. Besides, C-terminal fragment of PTHrP, known as OST, have shown to display anti-resorptive activity [18], also exhibiting osteogenic properties both in vitro and in vivo [19–24]. In addition, it was recently shown that OST coatings on several bioceramics and other biomaterials accelerates the healing of critical and non-critical long-bone defects in healthy and osteoporotic adult rabbits and rats [25–28]. Besides, our group has recently reported a synergistic effect of Zn^{2+} ions and OST, enhancing cell growth and osteogenic differentiation of pre-osteoblastic MC3T3-E1 cells in dense MBG disks [29], and of human MSCs in 3D meso-macroporous scaffolds analogous to those used in the present study [30]. These recent findings point to OST in conjunction with human MSC an attractive tool to be considered in bone tissue engineering approaches.

The aim of the present study was to design and evaluate an improved biomaterial, based on the above-mentioned scaffolds. Pristine meso-macroporous 82.2%SiO_2–10.3% CaO–3.3%P_2O_5–4.2%ZnO (mol %) (4ZN) scaffolds and after be loaded with OST (4ZN + OST), human MSC (4ZN + MSC) or both (4ZN + MSC + OST), were implanted for 3 months in defects (7.5 mm diameter, 12 mm depth) drilled in the distal femoral epiphysis of New Zealand rabbits.

2 Materials and methods

2.1 Synthesis and characterization of the scaffolds

Production and characterization of the scaffolds with composition 82.2%SiO_2–10.3%CaO–3.3%P_2O_5–4.2%ZnO (mol%) were described in detail in [30]. There, half-size analogous scaffolds (identical diameter, half height) were reported, investigating the loading and release of OST and the interaction with human MSC. MBGs were synthesized by the evaporation induced self-assembly technique, and MBG scaffolds as 3D structures were obtained by rapid prototyping 3D printer rapid prototyping equipment 3D Bioplotter™ (EnvisionTEC, Gladbeck, Germany) printer. The dimensions of the obtained cylindrical scaffolds were 7 mm diameter × 10 mm height. After its calcination at 700 °C, scaffolds were coated by immersion in 2.4% gelatin (GE) cross-linked with glutaraldehyde (GA) (0.05 w/v-%), giving rise to 4ZN scaffolds. The 4ZN scaffolds were exhaustively characterized in reference [26]. Briefly, interconnected macroporosity of MBG scaffolds and its chemical composition was analyzed in a JEOL JSM-6400

scanning electron microscope (SEM) (Tokyo, Japan) operating at 20 kV and equipped with an Oxford Instruments INCA Energy Dispersive X-ray (EDX) spectrometer. Mesoporous channel arrangement was evaluated by transmission electron microscopy (TEM) of crushed scaffolds carried out in a JEOL2100 electron microscope operating at 200 kV (Tokyo, Japan). To assess the composition of the scaffolds coated with GA cross-linked GE, Fourier transform infrared spectroscopy was performed in a Thermo Scientific Nicolet iS10 apparatus equipped with a SMART Golden Gate® attenuated total reflection ATR (Waltham, MA, USA). Thermogravimetric analyses were carried out with a Perkin-Elmer Pyris Diamond TG/DTA instrument, between 30 and 900 °C in air at a flow rate of 100 mL/min and a heating rate of 10 °C/min. The studied scaffolds were included into the culture medium (complete α-MEM, Minimum Essential Medium) for 10 days. The scaffolds were located in a 12 transwell plate in contact with the culture medium and 100 rpm shaking conditions. Culture medium was extracted every day to measure the zinc, calcium, phosphorous ions content in the solution by inductively coupled plasma/optical emission spectrometry (ICP/OES) using an OPTIMA 3300 DV Perkin Elmer device (Waltham, MA, USA).

2.2 Osteostatin loading and human mesenchymal cells seeding

4ZN scaffolds were incubated in 24-well plates with 1 mL of phosphate-buffered saline (PBS) at pH = 7.4 containing 100 nM OST (4ZN + OST). Materials were left overnight under stirring (400 rpm) at 4 °C. OST adsorption after 24 h was calculated based on the amount of peptide removed from the medium; whereas OST release was measured by soaking the peptide-loaded scaffolds in PBS also under stirring at 4 °C [30]. We found that the mean retention of OST by 4ZN scaffolds after 24 h of loading was 50%, equivalent to 0.70 µg OST/g scaffold. These loaded materials released (mean) 50% of loaded peptide to the surrounding medium within 1 h; 85% at 24 h; and virtually 100 % at 96 h (data not shown). Human MSC (Lonza, Walkersville, MD, USA) were withdrawn from the posterior iliac crest of the pelvic bone of normal volunteers. Human bone marrow cells are frozen in passage two and we used by passage five. Cell seeding in OST-loaded scaffolds was performed as described [30]. In short, scaffolds were placed into 24-well plates before human MSC seeding [31], purchased from Lonza (Walkersville, MD, USA). A suspension at $4{\bullet}10^5$ cells/scaffold was seeded on the top of each scaffold. After 30 min of seeding, each well was filled, until 2 mL, with MSC basal medium from Lonza (MSCBMTM), containing 10% fetal bovine serum, 1 mM L-Glutamine and 1% penicillin–streptomycin at 37 °C in a humidified atmosphere of 5% CO_2, and incubated for 2 days. Medium was replaced every day.

2.3 Surgical procedure

The study employed 12 female New Zealand rabbits, 6 months old and weighing on average 3.9 ± 0.3 kg. By means of a motorized drill, bone defects (7.5 mm diameter × 12 mm depth) were carved in the lateral aspect of both distal femoral epiphyses of all rabbits with continuous irrigation using physiological saline to prevent bone necrosis. Bone defects were then randomly filled during the surgical procedure with the scaffolds previously described. The animals continued the postoperative period in individual cages, under standard conditions (room temperature 20.0 ± 0.5 °C, relative humidity 55 ± 5% and illumination with a 12 h/12 h light/dark photoperiod), fed with full rabbit special fodder (Nantas®), given water ad libitum, and without movement restrictions. Surgery was accomplished under aseptic conditions by general anesthesia induced by subcutaneous injection of ketamine (25 mg/Kg) and medetomidine (0.5 mg/Kg), and intraspinal anesthesia. Intraoperative analgesia and anesthesia was maintained by means of Fentanyl and Lidocaine in saline serum up to a volume of 1 mL in the spinal canal. Ringer-Lactate intravenous solution was administered at a rate of 8 mL/Kg/h during the surgery.

Postoperative analgesia was maintained during 5 days by subcutaneous injection of Meloxicam 0.2 mg/Kg daily, and antibiotic prophylaxis was performed by means of two injections of Cefazoline (50 mg/Kg). Final euthanasia was carried out after 3 months of follow-up the animals and then 0.5 g of intravenous sodium thiopental were administered. The postoperative incidents during the experimental period are detailed in the supplementary material. Bone specimens obtained in the present study were processed for µCT and histological study. Some specimens were used in both studies, but the µCT was always previously performed.

The features of the created bone defects agreed with critical bone defects following the established requirements [32–36]. A gold standard group (control group) was not performed. Given the existence of numerous clinical and experimental evidences (of our research group and others) [37, 38] that the bone autograft is the gold standard in the treatment of bone defects, Ethical Commission for Animal Experimentation encouraged us to reduce the number of experimental animals to the minimum necessary, not including any control group. This recommendation avoids the unnecessary suffering of experimental animals, which is a common practice in experimental surgery. All procedures were carried out under Project License PI33/14 approved by the in-house Ethic Commission for Animal Experiments from the University of Zaragoza (Spain). The care and use

of animals were performed accordingly with the Spanish law (RD 53/2013) and international standards on animal welfare as defined by European Directive (2010/63/EU).

2.4 Radiographic and histological evaluation

After surgery, a radioscopic routine examination of the lateral vision of the operated femur was achieved to assess the implant placement. After sacrifice, the distal third of the bone specimens was extracted for histological study. Bones fixed with formaldehyde were dehydrated in alcohol graded series from 50 to 100%, and embedded in methyl methacrylate (Merck Schuchardt OHG, Germany). Sagittal sections obtained with a cutting–grinding system (EXAKT Apparatebeau GMBH, Norderstedt, Germany) were stained with hematoxylin and eosin (H&E) and Masson–Goldner trichrome for histological evaluation. Thickness of the grinding sections was 4–9 µm for H&E staining, and 5–19 µm for Masson–Goldner trichrome staining. Histological sections were examined with a Zeiss AxiokoP 40 microscope (Oberkochen, Germany) and microphotographs were obtained with a Zeiss AxioCam MRc5 camera. Light microscopy histological images with two different magnifications were shown. Images of panel **a** and **b** are of the same group, but those of **b** are not always close-up of **a** panel. For the sake of clarity, **b** panels showed representative images of the majority of the osteogenic effects observed in each group.

2.5 X-ray microtomography

The sample size requirements for the µCT study did not allow the introduction of the complete femur of rabbits. The distal third of the bone specimen from each rabbit were cut with a diamond disk and then scanned by high-resolution X-ray microtomography (µCT) in a BioScan nanoSPECT-CT (Dallas, TX, USA). The X-rays source is a continuously operating miniature micro focus X-ray tube with air filtration only. The detector is a high-resolution radiation-imaging device featuring a 1024 by 2048 pixels photodiode array with 48 µm pixel spacing. The scintillator screen is made of Gd2OI2S. The study was carried out with 65 kV of Tube Voltage, 1300 ms of Exposure time: 1300 ms, 360 projections and 0.5 pitches. The three-dimensional microstructural properties of the bone region of interest (Supplementary Fig. 1) were assessed by using the image software Vivoquant 2.0® (Invicro). The % of bone volume per total volume (BV/TV) around each scaffold (at 350 µm and 700 µm distance from the scaffold) was calculated.

2.6 Statistical analysis

Results were expressed as mean ± standard error of the mean (SEM). Statistical analysis was performed through nonparametric Kruskal–Wallis test and post hoc Dunn's test. A value of $p < 0.05$ was considered significant.

3 Results

The synthesis and characterization of this batch of scaffolds was previously described in detail by our research group [30]. There, three compositions were investigated, first ZnO-free and the other two containing respectively 4 and 5% ZnO. MBG loaded and unloaded with OST and its interactions with human MSC were also described. These in vitro results showed the added value of scaffolds to be containing simultaneously ZnO and OST because of the synergistic effect in the growth and osteogenic differentiation of MSC, being significantly more effective in 4% ZnO scaffolds. These results prompted us to investigate their behavior in an animal model. Scaffolds size were larger now (same diameter, double length) to fit the dimensions of the produced critical bone defect. As previously explained, four series of materials (pristine 4ZN, 4ZN + MSC, 4ZN + OST, and 4ZN + MSC + OST) were assessed in an animal model.

3.1 Implantation of 4ZN-based scaffolds in a bone defect in the rabbit femur

A critical bone defect (7.5 mm Ø × 12 mm depth) was created, in the lateral distal femoral epiphyses in all rabbits. Defect images, surgical implantation of 4ZN scaffold and its blood imbibition from the recipient bone bed are shown in Fig. 1a. To asses an implant placement, after surgical implantation, a radioscopic routine examination of the lateral vision of the operated femur was performed (Fig. 1b).

3.2 Necropsy study

Animals were sacrificed and femoral specimens were extracted and analyzed macroscopically (Fig. 2) before being processed for µCT and histological studies.

In the specimens treated with 4ZN scaffolds, the defect was filled with bone. Occasionally, the circular area of implantation, covered with newly formed bone, could be delimited. Alterations of normal femoral morphology were observed at the time of surgical implantation in two specimens due to the femoral condyle healed fracture. No scaffolds prominences or macroscopic remains were detected. Similarly, the treated bone defects appeared coated with bone in the specimens treated with 4ZN + MSC, perceiving macroscopic alterations. One specimen showed a healed fracture of the femoral condyle, detected from the surgical intervention, which altered the final femoral morphology. No morphological alterations were observed in the other specimens, although in one of them, a hemi-spherical bone

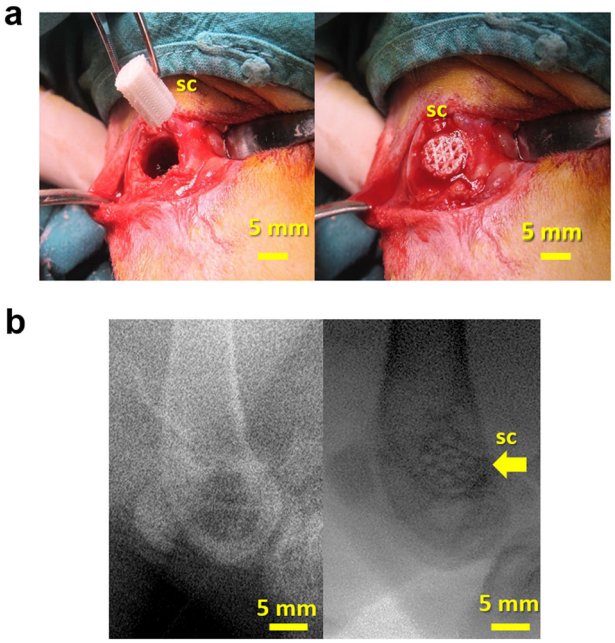

Fig. 1 **a** Digital image of the surgical implantation of 4ZN scaffold and its blood imbibitions of the recipient bone bed. **b** X-ray images of bone defect without and with a scaffold (sc) implanted in femoral epiphysis

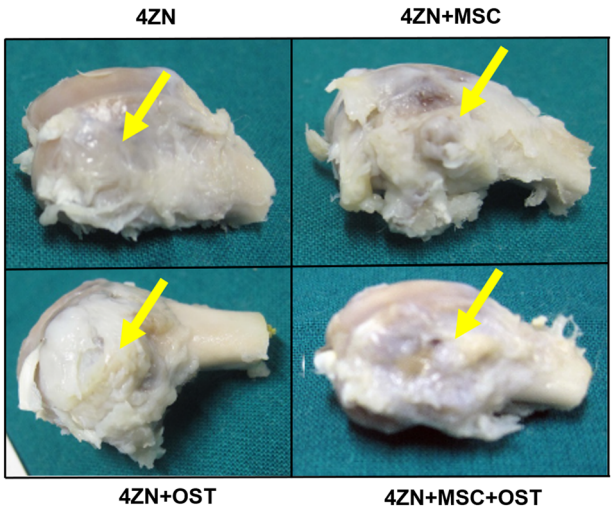

Fig. 2 Macroscopic appearance of bone specimens implanted 3 months with different scaffolds after necropsy. Arrows indicate the implants position

prominence was observed delimiting the circular area of implantation.

In the same way, bone defects treated with 4ZN + OST were covered with bone. Occasionally, a brownish color underlying the newly formed bone delimiting the implantation area, was detected. In one specimen there was an alteration, detected in the moment of the intervention, of the femoral morphology, secondary to the healed fracture of the femoral condyle.

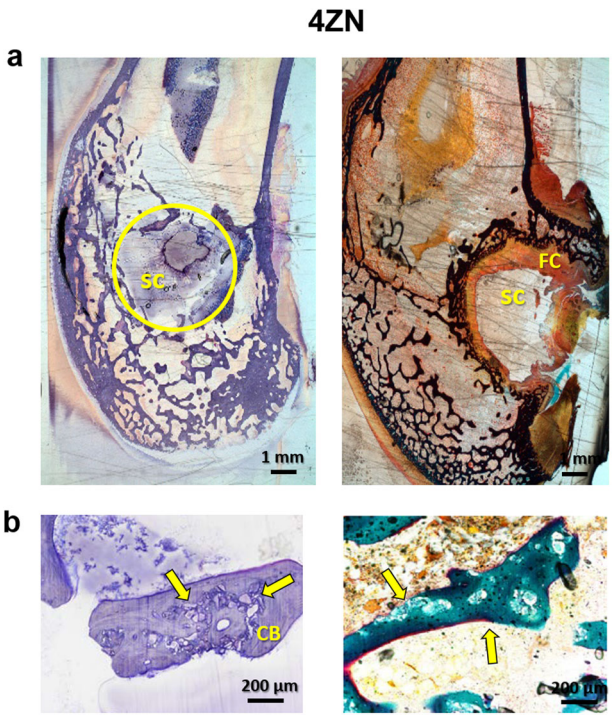

Fig. 3 Light microscopy from hematoxylin/eosin (**a** and **b**, left panels) and Masson–Goldner Trichrome (**a** and **b**, right panels) sagittal stained sections of the area surrounding 4ZN scaffolds (sc), containing newly formed bone at 3 months after production of a bone defect. Initial defect area is depicted with a yellow circle. Compact bone (CB) formation enveloping some not reabsorbed portions of the cylinder was observed (arrows). FC fibrous cap

As in the previous groups, bone defects treated with 4ZN + MSC + OST were covered with bone in all the specimens. The hemi-spherical bony prominence with brownish color delimiting the circular area of implantation was much more relevant than in the other groups.

3.3 Histological study

Implants were recognizable inside all bone specimens in methyl methacrylate blocks, but not always in the histological sections. It could be because of the procedure of polishing and sanding the histological sections of the EXAKT method, made before staining the cuts. Moreover, no sign of inflammation or adverse tissue reaction were observed around implants.

Figure 3 shows the histology results of the specimens treated with 4ZN scaffolds. In the histological sections, the implants and their limits were not clearly detected. Non-reabsorbed portions of the scaffolds were recognizable with a delimiting osteofibrous frame (Fig. 3a). In some compact bone formations, elements of irregular morphology and crystalline appearance were observed; suggesting bone neoformation in the remains of the implanted material

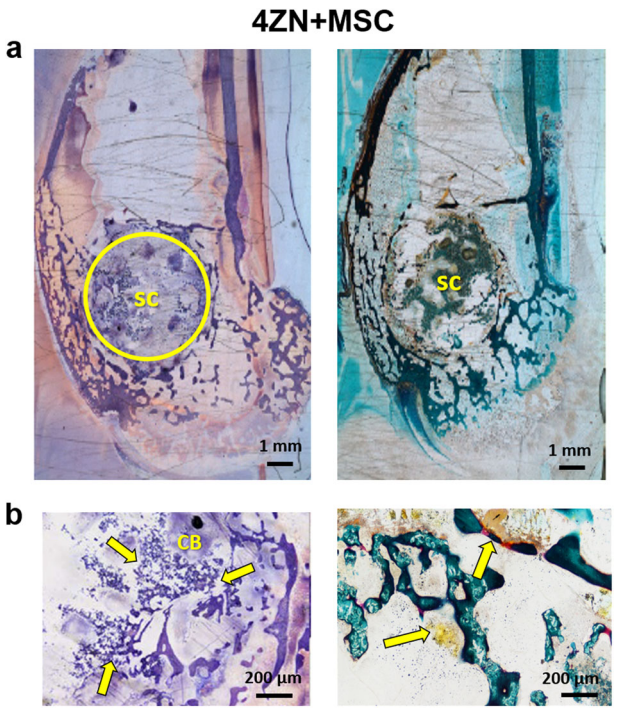

Fig. 4 Light microscopy from hematoxylin/eosin (**a** and **b**, left panels) and Masson–Goldner Trichrome (**a** and **b**, right panels) sagittal stained sections of the area surrounding 4ZN + MSC scaffolds (sc) containing newly formed bone at 3 months after production of a bone defect. Initial defect area is depicted with a yellow circle. In detail, crystalline material integrated into compact bone (CB) and fragmented without relation to the bone or delimited by dense masses of round cells (arrows)

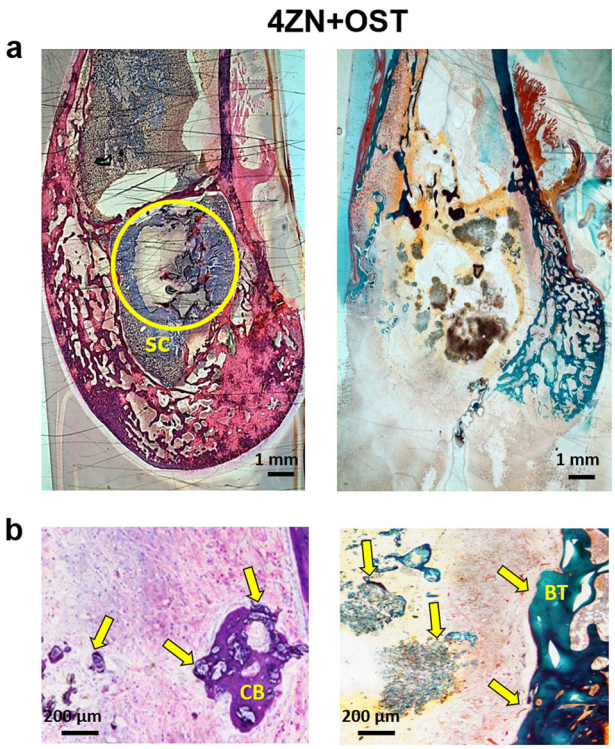

Fig. 5 Light microscopy from hematoxylin/eosin (**a** and **b**, left panels) and Masson–Goldner Trichrome (**a** and **b**, right panels) sagittal stained sections of the area surrounding 4ZN + OST scaffolds (sc) containing newly formed bone at 3 months after production of a bone defect. Initial defect area is depicted with a yellow circle. In detail, crystalline material integrated into compact bone (CB) and fragmented without relation to the bone or delimited by dense masses of round cells (arrows). BT Bone trabeculae

(Fig. 3b). The original structure of the implanted scaffolds was not clearly identified because of centripetal degradation.

Figure 4 shows the histology results of the specimens treated with 4ZN + MSC. The histological sections showed the implantation limits, being recognizable portions of the macroscopic structure of the ceramic cylinder surrounded by an osteofibrous cup. The presence of a relatively thick fibrous frame induced by 4ZN (Fig. 4a) was reduced by the presence of MSC (Fig. 4a).

Moreover, spicules of compact bone were observed around the implant area. These spicules, and the compact bone structure observed in some points, included a fragmented crystalline type material. At other points, this crystalline material seemed to be integrated into compact bone. In others, it appeared fragmented without having any relation to the bone or delimited by dense masses of cells. These findings suggest greater bioactivity and osseointegration (Fig. 4b). As observed in the previous group, implants were recognizable inside the bone specimens in methyl methacrylate blocks with modifications of its peripheral morphology.

In specimens treated with 4ZN + OST, implants and their limits were not clearly appreciated, except in one of the specimens investigated. An osteofibrous frame could be observed delimiting the place of implantation, with remaining areas of crystalline material inside compact bone (Fig. 5a, b). Therefore, OST loading in 4ZN scaffolds promoted the proliferation of osteogenic precursor cells and connective tissue formation. The fibrous frame was reduced in these specimens compared with pristine 4ZN scaffolds (Fig. 5a). In specimens treated with 4ZN + MSC + OST, remains of the degraded implants were clearly identified with less sharpness and surrounded by a thin osteofibrous frame (Fig. 6a). The combination of OST and MSC in 4ZN induced a neoformed bone trabeculae in intimate contact suggesting osseointegration (Fig. 6b).

3.4 µCT study

Bone repair and bone tissue response to the implanted scaffolds, in combination or not with MSC and/or OST, were also examined by µCT in the scaffold-tissue interface and in the peripheral area of the implant (Fig. 7, top).

For the specimens treated with 4ZN, degraded implants were observed with variable loss of their initial morphology,

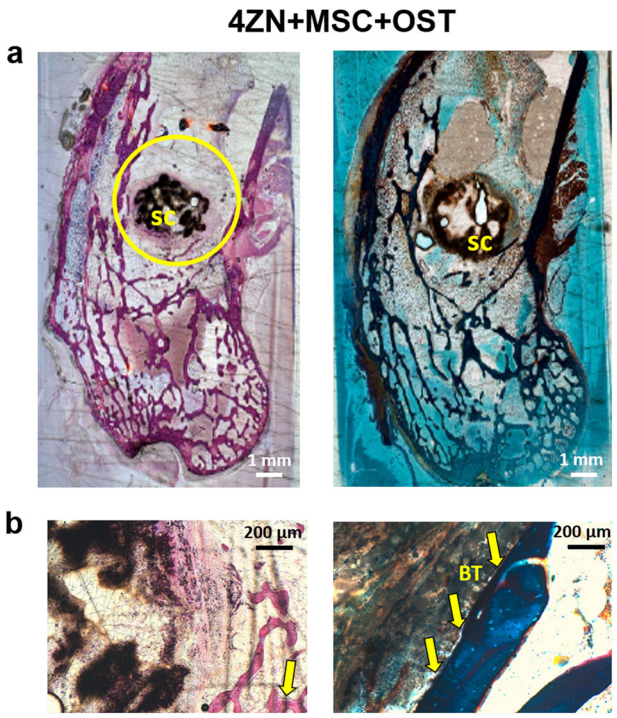

Fig. 6 Light microscopy from hematoxylin/eosin (**a** and **b**, left panels) and Masson–Goldner Trichrome (**a** and **b**, right panels) sagittal stained sections of the area surrounding 4ZN + MSC + OST scaffolds (sc) containing newly formed bone at 3 months after production of a bone defect. Initial defect area is depicted with a yellow circle. In detail, bone trabeculae (BT) in intimate contact with the degraded material suggesting osteointegration (arrows)

surrounded by less radiological density area, probably due to peripheral resorption. In some portions of its surface, the appearance of bony trabeculae was detected contouring the implant as a bone frame. In the specimens treated with 4ZN + MSC, remains of the degraded implants were present in a more homogeneous form than observed in the previous group. Moreover, it was also detected a lower peripheral radiological density area which seems to correspond to the centripetal resorption of the implants. As in the previous group, portions of bone framing of the implants surrounding the centripetal degradation zone were observed. In a similar way than detected in other groups, specimens treated with 4ZN + OST showed greater centripetal degradation, although not having homogeneous implants. It was also appreciable a peripheral halo of lower radiological density, delimited by a bony framework. In the specimens treated with 4ZN + MSC + OST scaffolds, the degradation was greater than in previous groups, with also centripetal predominance although not following a homogeneous pattern. Radio dense bands that could correspond to newly formed bone were observed with a lower peripheral density zone around the remains of the implants and also delimited by a bony frame.

The osteoconductive and osteoinductive effects of OST and MSC loaded into 4ZN scaffolds, observed in µCT images and in histological analysis, were confirmed by the quantification of the % bone volume per total volume (BV/TV) in the nine bone specimens investigated. We found that OST loaded scaffolds or MSC decorated scaffolds significantly increased % BV/TV, compared to pristine 4ZN. This positive effect was more evident when the scaffolds were combined with OST and MSC together (Fig. 7 bottom). In terms of percentage, a greater BV/TV (35%) were measured in scaffolds combined with OST and MSC, than in MSC decorated scaffolds (26%) or OST loaded scaffolds (28%). Finally, 4ZN exhibited the lower BV/TV value (15%).

4 Discussion

It must be taken into account that an ideal bone substitute should be osteogenic, biocompatible, bio absorbable, capable of providing structural support and release biologically active substances. Moreover, it must be easy handling in clinic with an adequate cost-benefit ratio. The scaffolds designed for this study showed the composition, dimensions, and porosity desired to treat the investigated bone defect. Due to this, designed scaffold were optimal for bone tissue engineering application. Moreover, they were readily loaded with OST and/or MSC.

Necropsy, histological and 3 months of implantation µCT results, suggested that all the scaffolds assessed allow bone growth over their surface, by a mesenchymal cells recruitment process from the surrounding bone and its subsequent transformation in bone-forming cells as consequence of local bioactivity [2, 7, 37, 38]. According to Shors [39] bone formation over a bioactive implant in ideal conditions, should be predominantly of membranous type. In our study, bone and fibrous tissue were observed over all implants but without chondral cells, as evidence of an ideal membranous type of bone growth. Our observations supported the evidence of bone viability where implants were fixed, one of the three requirements of Shors [39] "triad of osteoconduction": stability, viability, and proximity. The healing of critical bone defects demonstrated the viability of the epiphyseal and metaphyseal bone to facilitate the osseointegration process of the tested scaffolds. As previously mentioned, EXAKT band and polishing saw system have specific characteristics that can vary the observation and evaluation of the stains compared to the characteristics observed in deparaffinized sections. The inflammatory process is a combination of clinical, tissue, cellular, and biochemical phenomena. In experimental surgery we can assess the clinical aspects of the inflammatory process during clinical postoperative follow-up, necropsy, and

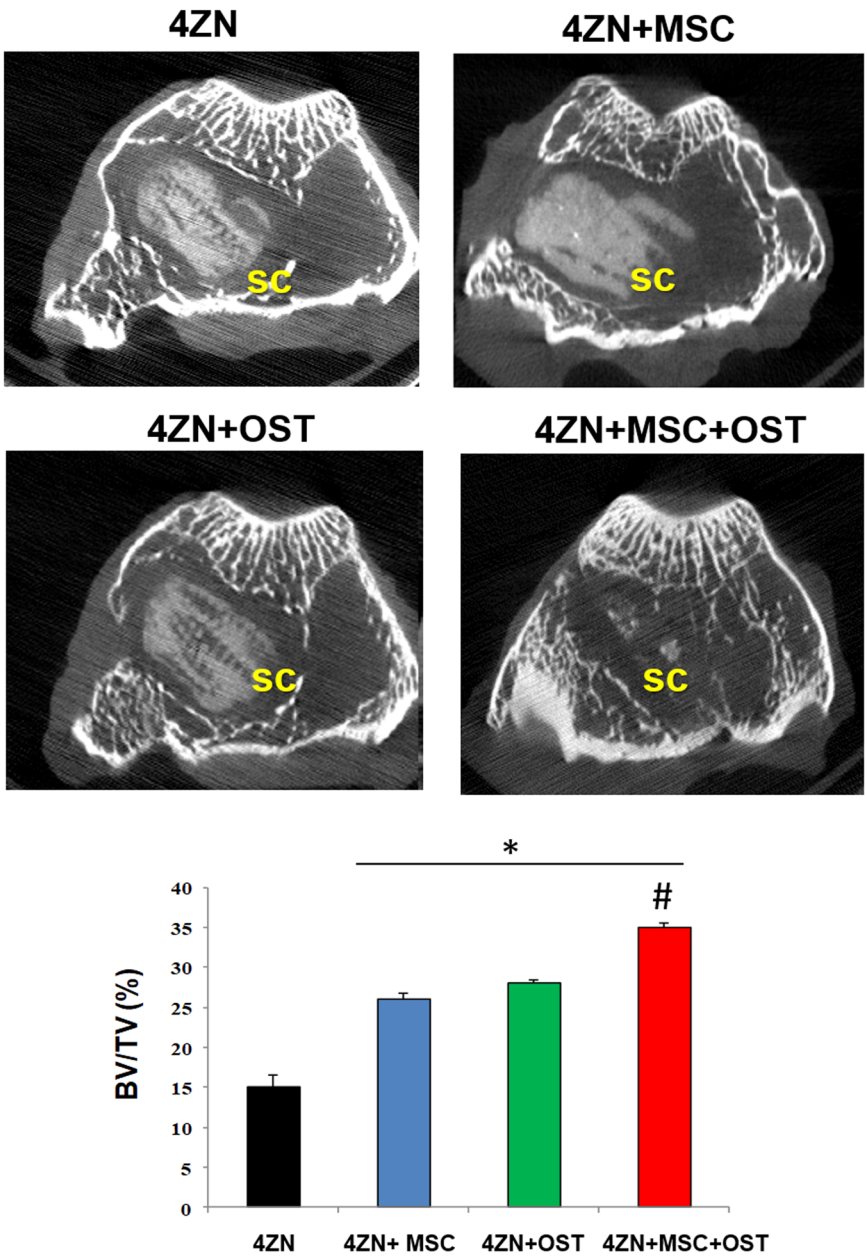

Fig. 7 Representative μCT projection images of the area surrounding the different scaffolds (sc), containing newly formed bone 3 months after production of a bone defect. At the bottom of the figure trabecular bone volume per total volume (BV/TV) measured by μCT around the different type of scaffolds in the bone defect. Results are mean ± SE. $^{*}p < 0.05$ vs. 4ZN scaffold; $^{\#}p < 0.05$ vs. 4ZN + MSC and 4ZN + OST scaffolds

postmortem histological study, which supported an adequate in vivo bioactivity [37, 38]. No inflammatory abnormalities were observed other than the usual ones of a satisfactory postoperative period, nor during the autopsy.

Evidence of degradation and absorption of implanted cylinders was clearly observed following the conditions of Bauer and Muschler [40] for bone remodeling of a synthetic bone graft substitute, with progressive growth of bone and fibrous tissue to heal the bone defect. This positive effect on bone growth and remodeling was previously observed with similar bioglass scaffolds that contain polypeptides in vivo [2, 41, 42], and by our group [25–27, 37, 38], with others materials in critical and non-critical bone defects, suggesting a process of mesenchymal cells recruitment of surrounding tissues and subsequent transformation in bone-forming cells. The size of critical bone defects created in this study according to the standard requirements [32–36] may explain the occasional posterior bed bone marginal fractures observed during implantation, although without instability of the implanted scaffold. The healing of these intraoperative fractures explains the morphological alterations observed in some specimens during the necropsy.

Several scaffold preparation techniques can be found in the literature. Some of them have been adapted from other research areas or have been achieved through modification of traditional techniques [43–45]. Moldable and 3D printable composite scaffolds are an interesting type of materials that can find suitable application as fillers in bone

reconstructive surgery and in the treatment of particular clinical and experimental situations [2, 27, 28, 43, 45, 46]. The design of scaffolds for bone regeneration based on biodegradable polymers must consider the polymer and the resulting scaffold mechanical strength, and even its shape, according the place of implantation and clinical or surgical requirements. Bones must withstand high pressures and may be necessary the scaffold to present high mechanical strength, including both compressive and tensile strength. These properties are necessary until the regenerated tissue owns sufficient mechanical strength itself [36]. The presence of biological signals as growth factors, OST or zinc inside of the scaffold, should improves bone regeneration, being an important aid when, in certain clinical or experimental situations, natural bone repair is not enough [1, 2, 15, 25, 26, 45–47]. Growth factor instability can be overcome through loading it into a carrier that protects the protein and promotes its controlled release hence prolongs its activity whenever administered into the body [43, 45]. In this regard, OST displays some important advantages compared with other osteogenic proteins, as BMPs for example [2]. This peptide has shown to display anti-resorptive activity but also osteogenic properties both in vitro and in vivo, while BMPs exerts osteogenic features but can be adipogenic at high doses. These positive effects of OST are specific of bone cells and keratinocytes, while BMP-2 effects are pleiotropic, acting on many tissues and activating the immune system [2]. OST is a small pentapeptide easy to immobilize in different biomaterials, active at low concentrations (<nM) and very important for local applications. Conversely, BMP-2 has a larger molecular weight, making more difficult to immobilize in materials, and higher concentrations (>nM) are required to induce osteogenic effects [2].

In a previous study, we demonstrated in vitro for the first time, a synergistic effect of zinc and OST to enhance MSC cell growth and osteogenic differentiation, suggesting its potential use in bone tissue engineering applications [30]. Here, the use of MGB scaffolds doped with 4.2% ZnO, loaded with OST and decorated with MSC significantly improved bone regeneration, reducing the fibrous cup induced by 4ZN scaffolds, providing a novel and interesting insight in the field of bone regeneration. These results are in concordance with previous studies of our group where OST loading on different bioceramics and other biomaterials improves the healing of critical and non-critical long-bone defects in healthy and osteoporotic adult rabbits and rats [25–28, 48]. Thus, OST, in combination or not with MSC, increased in vitro osteogenic capacity of Zn^{2+} ions enriched materials, as we demonstrated by increasing % BV/TV, suggesting the potential of this method in bone tissue engineering applications [2]. Moreover, the release of Zn^{2+} ions from the scaffold is thought to stimulate the osteoblastic bone building process and reduce the osteoclastic resorption process [29, 44, 47, 49–51].

The histological findings and the μCT images point toward a centripetal degradation of the implants and bone repair with healing of the bone defect predominantly of membranous type in the same direction. In our study, 4ZN scaffolds showed evidence of osseointegration with a progressive loss of its initial morphology, even though all the studied groups were inhomogeneous, without complete resorption after three months of implantation. These qualitative findings are supported by the measured % BV/TV in the four different scaffold combinations. Similar findings have been described in comparative experimental models of bone defect, although those were not critical and with different follow-up time [25, 26].

As we previously mentioned, certain bone defects that have scarce or null capacity of regeneration need to be treated with bone grafts that favored the repair process. For this goal, bone autografts are the gold standard, but these grafts have limitations in obtaining osseous tissue needed and the morbidity in the donor area. Thus, there is an urgent necessity to design biomaterials capable of substitute autografts without its limitations. Several research groups face this problem by using bone tissue engineering principles based on three-dimensional scaffolds loaded with biomolecules and decorated with mesenchymal cells. Nevertheless, our present study has been the first to investigate bioactive mesoporous glasses, improved by adding an osteogenic and bactericidal ion such as zinc and an osteogenic and anti-resorptive pentapeptide (OST), in addition to human-mesenchymal bone marrow cells. In addition, further in vivo studies at longer experimental times and in superior animals as sheep or pig, will be necessary before the clinical trials that yield to the clinical use of these materials. However, our results suggest that the loading of Zn-containing MBG scaffolds with MSC and OST significantly improves the bone healing because of inducing neo-formed bone trabeculae in intimate contact with a higher rate of implants degradation, increasing % BV/TV and reducing the fibrous frame induced by the unloaded scaffolds.

5 Conclusions

The osteogenic capability of 3D meso-macroporous biomaterials based on ZnO-enriched mesoporous bioactive glass scaffolds combined with OST and human MSCs were evaluated after 3 months of implantation in New Zealand rabbits. The present study showed for the first time that the healing process in a critical bone defect was clearly improved by the implantation of these scaffolds investigated as carriers of biological signals (OST) and bone-forming

cells, compared with non-loaded ZnO-enriched scaffold. Therefore, biomaterials here investigated promote advantageous local biological conditions leading to very remarkable results in bone regeneration field. Given the safety, ease of handling and low expense, translation of this bio-functional biomaterial into clinical bone reconstructive surgery of personalized implants is of interest to the scientific orthopedic community.

Acknowledgements This research was funded by Instituto de Salud Carlos III, grant number PI15/00978 co-financed with the European Union FEDER funds, the European Research Council, Advanced Grant Verdi-Proposal No. 694160 (ERC-2015-AdG).

Author contributions Conceptualization, DL, JGA, and AJS; Funding acquisition, MVR and AJS; Investigation, DL, CH, SSS, EGP, and AGB; Methodology, JGA, CH, EGP, AGB and JCD; Supervision, JGA, MVR and AJS; Validation, DL and JGA; Visualization, DL and JGA; Writing–original draft, DL and JGA; Writing–review & editing, DL, JGA, CH, SSS, and AJS. All authors have read and agreed to the published version of the paper.

Compliance with ethical standards

Conflict of interest The authors declare that they have no conflict of interest.

Publisher's note Springer Nature remains neutral with regard to jurisdictional claims in published maps and institutional affiliations.

References

1. Bose S, Roy M, Bandyopadhyay A. Recent advances in bone tissue engineering scaffolds. Trends Biotechnol. 2012;30:546–54.
2. Salinas AJ, Esbrit P, Vallet-Regí M. A tissue engineering approach based on the use of bioceramics for bone repair. Biomater. Sci. 2013;1:40–51.
3. Wu SL, Liu XM, Yeung WK, Liu CS, Yang XJ. Biomimetic porous scaffolds for bone tissue engineering. Mater Sci Eng R-Rep. 2014;80:1–36.
4. Hench LL, Splinter RJ, Allen WC, Greenlee TK. Bonding mechanisms at the interface of ceramic prosthetic materials. J Biomed Mater Res Symp. 1971;2:117–41.
5. Li R, Clark AE, Hench LL. An investigation of bioactive glass powders by sol-gel processing. J Appl Biomater. 1991;2:231–9.
6. Yan X, Yu C, Zhou X, Tang J, Zhao D. Highly ordered mesoporous bioactive glasses with superior in vitro bone forming bioactivities. Angew Chem Int Ed. 2004;43:5980–4.
7. Vallet-Regí M, Salinas AJ, Arcos D. Tailoring the structure of bioactive glasses: from the nanoscale to macroporous scaffolds. Int J App l Glass Sci. 2016;7:195–205.
8. Vallet-Regí M, Ragel CV, Salinas AJ. Glasses with medical applications. Eur J Inor Chem. 2003;1:1029–42.
9. Izquierdo-Barba I, Arcos D, Sakamoto Y, Terasaki O, López-Noriega A, Vallet-Regí M. High-performance mesoporous bioceramics mimicking bone mineralization. Chem Mater. 2008;20:3191–8.
10. Hench LL. Genetic design of bioactive glass. J Eur Ceram Soc. 2009;29:1257–65.
11. Kaya S, Cresswell M, Boccaccini AR. Mesoporous silica-based bioactive glasses for antibiotic-free antibacterial applications. Mater Sci Eng C-Mater. 2018;83:99–107.
12. Yu YQ, Jin GD, Xue Y, Wang DH, Liu XY, Sun J. Multifunctions of dual Zn/Mg ion co-implanted titanium on osteogenesis, angiogenesis and bacteria inhibition for dental implants. Acta Biomater. 2017;49:590–603.
13. Gittard SD, Perfect JR, Monteiro-Riviere NA, Wei W, Jin CM, Narayan RJ. Assessing the antimicrobial activity of zinc oxide thin films using disk diffusion and biofilm reactor. Appl Surf Sci. 2009;255:5806–11.
14. Lozano D, Manzano M, Doadrio JC, Salinas AJ, Vallet-Regí M, Gómez-Barrena E, et al. Osteostatin-loaded bioceramics stimulate osteoblastic growth and differentiation. Acta Biomater. 2010;6:797–803.
15. Esbrit P, Alcaraz MJ. Current perspectives on parathyroid hormone (PTH) and PTH-related protein (PTHrP) as bone anabolic therapies. Biochem Pharmacol. 2013;85:1417–23.
16. Datta NS, Abou-Samra AB. PTH and PTHrP signalling in osteoblasts. Cell Signal. 2009;21:1245–54.
17. Lozano D, De Castro LF, Dapía S, Andrade-Zapata I, Manzarbeitia F, Alvarez-Arroyo MV, et al. Role of Parathyroid Hormone-Related Protein in the Decreased Osteoblast Function in Diabetes-Related Osteopenia. Endocrinology. 2009;150:2027–35.
18. Fenton AJ, Kemp BE, Hammonds RG, Mitchelhill K, Moseley JM, Martin TJ, et al. A potent inhibitor of osteoclastic bone resorption within a highly conserved pentapeptide region of parathyroid hormone-related protein, PTHrP. Endocrinology. 1991;129:3424–6.
19. Cornish J, Callon KE, Nicholson GC, Reid IR. Parathyroid hormone-related protein (107–139) inhibits bone resorption in vivo. Endocrinology. 1997;138:1299–304.
20. Cornish J, Callon KE, Lin C, Xiao C, Moseley JM, Reid IR. Stimulation of osteoblast proliferation by C-terminal fragments of parathyroid hormone-related protein. J Bone Mine Res. 1999;14:915–22.
21. Lozano D, Fernández de Castro LF, Portal-Núñez S, López-Herradón A, Dapía S, Gómez-Barrena E, et al. The C-terminal fragment of parathyroid hormone-related peptide promotes bone formation in diabetic mice with low-turnover osteopenia. Br J Pharmacol. 2011;162:1424–38.
22. Rihani-Basharat S, Lewinson D. PTHrP(107-111) Inhibits In Vivo Resorption that was Stimulated by PTHrP(1-34) When Applied Intermittently to Neonatal Mice. Calcif Tissue Int. 1997;61:426–8.
23. Fenton AJ, Kemp BE, Ken GN, Moseley JM, Zheng MH, Rowe DJ, et al. A Carboxyl-Terminal Peptide from the Parathyroid Hormone-Related Protein Inhibits Bone Resorption by Osteoclasts. Endocrinology. 1991;129:1762–8.
24. De Gortázar AR, Alonso V, Alvarez-Arroyo MV, Esbrit P. Transient Exposure to PTHrP (107–139) Exerts Anabolic Effects through Vascular Endothelial Growth Factor Receptor 2 in Human Osteoblastic Cells in Vitro. Calcif Tissue Int. 2006;79:360–9.
25. Trejo CG, Lozano D, Manzano M, Doadrio JC, Salinas AJ, Dapía S, et al. The osteoinductive properties of mesoporous silicate coated with osteostatin in a rabbit femur cavity defect model. Biomaterials. 2010;31:8564–73.
26. Lozano D, Trejo CG, Gómez-Barrena E, Manzano M, Doadrio JC, Salinas AJ, et al. Osteostatin-loaded onto mesoporous ceramics improves the earlyphase of bone regeneration in a rabbit osteopenia model. Acta Biomater. 2012;8:2317–23.
27. Lozano D, Sánchez-Salcedo S, Portal-Nuñez S, Vila M, López-Herradón A, Ardura JA, et al. Parathyroid hormone-related protein (107-111) improves the bone regeneration potential of gelatin-glutaraldehyde biopolymer-coated hydroxyapatite. Acta Biomater. 2014;10:3307–16.
28. Ardura JA, Portal-Núñez S, Lozano D, Gutiérrez-Rojas I, Sánchez-Salcedo S, López-Herradón A, et al. Local delivery of parathyroid hormone-related protein-derived peptides coated onto a hydroxyapatite-based implant enhances bone regeneration in old and diabetic rats. J Biomed Mater Res A. 2016;104:2060–70.

29. Pérez R, Sanchez-Salcedo S, Lozano D, Heras C, Esbrit P, Vallet-Regí M, et al. Osteogenic Effect of ZnO-Mesoporous Glasses Loaded with Osteostatin. Nanomaterials. 2018;8:592.
30. Heras C, Sanchez-Salcedo S, Lozano D, Peña J, Esbrit P, Vallet-Regi M, et al. Osteostatin potentiates the bioactivity of mesoporous glass scaffolds containing Zn2+ ions in human mesenchymal stem cells. Acta Biomater. 2019;89:359–71.
31. Thorpe AA, Creasey S, Sammon C, Le Maitre CL. Hydroxyapatite nanoparticle injectable hydrogel scaffold to support osteogenic differentiation of human mesenchymal stem cells. Eur Cell Mater. 2016;32:1–23.
32. Lasanios NG, Kanakaris NK, Giannoudis PV. Current management of long bone large segmental defects. J Orthop Trauma. 2009;24:149–63.
33. Miño-Fariña N, Muñoz-Guzón F, López-Peña M, Ginebra MP, del Valle-Fresno S, Ayala D, et al. Quantitative analysis of the resorption and osteoconduction of a macroporous calcium phosphate bone cement for the repair of a critical size defect in the femoral condyle. Vet J. 2009;179:264–72.
34. Reichert JC, Saifzadeh S, Wullschleger ME, Epari DR, Schütz MA, Duda GN, et al. The challenge of establishing preclinical models for segmental bone defect research. Biomaterials. 2009;30:2149–63.
35. Cacchioli A, Spaggiari B, Ravanetti F, Martini FM, Borghetti P, Gabbi C. The critical size bone defect: morphological study of bone healing. Ann Fac Medic Vet Parma. 2006;26:97–100.
36. Cugala Z, Gogolewski S. Regeneration of segmental diaphyseal defects in sheep tibiae using resorbable polymeric membranes: a preliminary study. J Orthop Trauma. 1999;13:187–95.
37. Gil-Albarova J, Garrido-Lahiguera R, Salinas AJ, Roman J, Bueno-Lozano AL, Gil-Albarova R, et al. The in vivo performance of a sol–gel glass and a glass-ceramic in the treatment of limited bone defects. Biomaterials. 2004;25:4639–45.
38. Gil-Albarova J, Vila M, Badiola-Vargas J, Sánchez-Salcedo S, Herrera A, Vallet-Regi M. In vivo osteointegration of three-dimensional crosslinked gelatin-coated hydroxyapatite foams. Acta Biomater. 2012;8:3777–83.
39. Shors EC. Coraline bone graft substitutes. Orthop Clin North Am. 1999;30:599–613.
40. Bauer TW, Muschler GF. Bone graft materials: an overview of the basic science. Clin Orthop. 2000;71:10–27.
41. Gao T, Aro HT, Ylänen H, Vuorio E. Silica-based bioactive glasses modulate expression of bone morphogenetic protein-2 mRNA in Saos-2 osteoblasts in vitro. Biomaterials. 2001;22:1475–83.
42. Wai-Ching L, Irina SR, Rikin P, Ming CL, Velez M, Chu TM. The effects of 3D bioactive glass scaffolds and BMP-2 on bone formation in rat femoral critical size defects and adjacent bones. Biomed Mater. 2014;9:045013.
43. Caramella C, Conti B, Modena T, Ferrari F, Bonferoni MC, Genta I, et al. Controlled delivery systems for tissue repair and regeneration. J Drug Deliv Sci Technol. 2016;32:206–28.
44. Liu D, Nie W, Li D, Wang W, Zheng L, Zhang J, et al. 3D printed PCL/SrHA scaffold for enhanced bone regeneration. Chem Eng J. 2019;362:269–79.
45. Begam H, Nandi SK, Chanda A, Kundu B. Effect of bone morphogenetic protein on Zn-HAp and Zn-HAp/collagen composite: a systematic in vivo study. Res Vet Sci. 2017;115:1–9.
46. Dias MR, Guedes JM, Flanagan CL, Hollister SJ, Fernandes PR. Optimization of scaffold design for bone tissue engineering: a computational and experimental study. Med Eng Phys. 2014;36:448–57.
47. Barceloux DGJ. Zinc. Toxicol, Clin Toxicol. 1999;37:279–92.
48. van der Stok J, Lozano D, Chai YC, Amin YS, Bastidas CAP, Verhaar JA, et al. Osteostatin-coated porous titanium can improve early bone regeneration of cortical bone defects in rats. Tissue Eng Part A. 2015;21:1495–506.
49. Xie E, Hu Y, Chen X, Bai X, Li D, Ren L, et al. In vivo bone regeneration using a novel porous bioactive composite. Appl Surf Sci. 2008;255:545–7.
50. Hadley KB, Newman SM, Hunt JR. Dietary zinc reduces osteoclast resorption activities and increases markers of osteoblast differentiation, matrix maturation, and mineralization in the long bones of growing rats. J Nutr Biochem. 2010;2:297–303.
51. Yamaguchi M, Weitzmann MN. Zinc stimulates osteoblastogenesis and suppresses osteoclastogenesis by antagonizing NF-kB activation. Mol Cell Biochem. 2011;355:179–86.